PALEOCEANOGRAPHY, VOL. 15, NO. 6, PAGES 625-641 DECEMBER 2000

Ocean thermohaline circulation and sedimentary $^{231}Pa/^{230}Th$ ratio

Olivier Marchal

Climate and Environmental Physics, Physics Institute, University of Bern, Bern

Roger François

Department of Marine Chemistry and Geochemistry, Woods Hole Oceanographic Institution
Woods Hole, Massachusetts

Thomas F. Stocker and Fortunat Joos

Climate and Environmental Physics, Physics Institute, University of Bern, Bern

Abstract. Holocene sediments from the Atlantic are characterized by $^{231}Pa/^{230}Th$ ratios below the production ratio of the two radionuclides in the water column (0.093), whereas Holocene sediments from the Southern Ocean have $^{231}Pa/^{230}Th > 0.093$. This pattern of ^{231}Pa deficit and excess was ascribed to southward ^{231}Pa export from the Atlantic by the Atlantic thermohaline circulation (THC) as Pa is scavenged less efficiently by marine particles and more effectively transported by the THC than Th. The same pattern is observed in deposits of the Last Glacial Maximum (LGM), which led to a previous contention that the THC strength did not vary markedly through the last glacial termination. Here we embed a description of trace metal scavenging into a zonally averaged, circulation-biogeochemistry ocean model to explore the sensitivity of $^{231}Pa/^{230}Th$ in Atlantic and Southern Ocean sediments to THC changes. Our results show that the production of biogenic opal (which, unlike other marine particles, poorly fractionates Th and Pa) in the Southern Ocean water column determines the spatial pattern of the sensitivity. Also, $^{231}Pa/^{230}Th$ increases in the North Atlantic but changes little in the South Atlantic and decreases in the Southern Ocean as THC is reduced. The mean $^{231}Pa/^{230}Th$ of the whole Atlantic is therefore less sensitive to THC changes than the mean $^{231}Pa/^{230}Th$ of the North Atlantic. The current uncertainties in Atlantic mean $^{231}Pa/^{230}Th$ are too large to rule out a twofold reduction of the THC at the LGM. However, the increase in North Atlantic mean $^{231}Pa/^{230}Th$ simulated in response to a twofold THC reduction is larger than the observed change in the North Atlantic mean $^{231}Pa/^{230}Th$ from the LGM to Holocene. Comparing this change with the modeled sensitivity of North Atlantic $^{231}Pa/^{230}Th$ to THC variations indicates that the THC at the LGM could not have been reduced by $> 30\%$ of its present strength. Experiments of transient THC changes indicate that high-resolution $^{231}Pa/^{230}Th$ records from North Atlantic sediments could also document thermohaline oscillations on century-to-millennial timescales.

1. Introduction

Radioisotopes ^{231}Pa (half-life of 32.5 kyr) and ^{230}Th (75.2 kyr) are naturally occurring, produced from the α decay of ^{235}U and ^{234}U, respectively. The activity of U is essentially uniform in the ocean [*Chen et al.*, 1986], with $A_{U-235} \simeq 108$ disintegrations per minute per cubic meter of water (dpm m^{-3}) and $A_{U-234} \simeq 2750$ dpm m^{-3}. Thus ^{231}Pa and ^{230}Th are produced at a constant rate in the water column, according to a production ratio $\beta_{Pa-231}/\beta_{Th-230} = (\lambda_{Pa-231} A_{U-235})/(\lambda_{Th-230} A_{U-234}) = 0.093$ (where λ is the radiodecay constant). The activity ratios A_{Pa-231}/A_{U-235} ($\sim 10^{-3}$) and A_{Th-230}/A_{U-234} ($\sim 10^{-4}$) are well below unity, pointing to very strong radioactive disequilibria in ocean waters. The process responsible for these disequilibria is scavenging, i.e., the adsorption of ^{231}Pa and ^{230}Th onto settling particles and subsequent removal to the sediments [*Anderson et al.*, 1983a, 1983b; *Bacon*, 1988]. The affinity of marine particles is generally higher for thorium than for protactinium. This is illustrated by the fractionation factor $f = (A_{Th-230}/A_{Pa-231})_p/(A_{Th-230}/A_{Pa-231})_d$ (where p stands for particulate and d is for dissolved), which typically approaches 10 in ocean waters [*Nozaki and Nakanishi*, 1985; *Walter et al.*, 1997]. Hence the mean residence time with respect to scavenging in deep waters is substantially longer for ^{231}Pa (~ 200 years) than for ^{230}Th (~ 30 years) [*Yu et al.*, 1996].

Paper number 2000PA000496.
0883-8305/00/2000PA000496$12.00

Because of this difference in particle reactivity the $^{231}Pa/^{230}Th$ ratio of deep-sea sediments exhibits a pronounced geographic variability (the $^{231}Pa/^{230}Th$ ratios considered here are corrected for ^{231}Pa and ^{230}Th supported by U isotopes present in the sediment mineral lattices and for radiodecay since the time of deposition). The mean residence time of ^{231}Pa with respect to scavenging is comparable to the mean ventilation time of the modern deep Atlantic, which was estimated to $\sim$ 100 years [*Broecker*, 1979] or $\sim$ 275 years [*Stuiver et al.*, 1983]. A relatively large fraction of the ^{231}Pa produced in the Atlantic can thus be exported to the Southern Ocean by the southward flowing North Atlantic Deep Water (NADW). This is reflected in the $^{231}Pa/^{230}Th$ ratio of Atlantic sediments deposited during the Holocene (0–10 kyr B.P.), which is most generally below the production ratio of the two radionuclides in the water column [*Yu et al.*, 1996; *Walter et al.*, 1999]. *Yu et al.* [1996] estimated that $\sim$ 45% of the ^{231}Pa produced in the Atlantic basin (north of 50°S) is exported today to the Southern Ocean, compared to only $\sim$ 15% for ^{230}Th (the exported ^{231}Pa and ^{230}Th are primarily in dissolved form, which constitutes the bulk of ^{231}Pa and ^{230}Th in seawater [e.g., *Walter et al.*, 1997; *Vogler et al.*, 1998]). Sediments from the Southern Ocean, on the other hand, have a $^{231}Pa/^{230}Th$ ratio higher than 0.093 [*Walter et al.*, 1999], suggesting that the ^{231}Pa originating from the Atlantic is deposited, at least partly, in the Southern Ocean.

A pattern of ^{231}Pa depletion in Atlantic sediments and ^{231}Pa enrichment in Southern Ocean sediments is also observed for the Last Glacial Maximum (LGM) at $\sim$ 21 kyr B.P. [*Yu et al.*, 1996]. This led *Yu et al.* [1996] to conclude that the net, interbasin transfer of ^{231}Pa and thus NADW export to the Southern Ocean during the LGM and Holocene were similar. This conclusion conflicts with benthic $\delta^{13}C$ and Cd/Ca records from North Atlantic sediments and benthic $\delta^{13}C$ records from Southern Ocean sediments, which point to reduced NADW production during the LGM (for a review, see *Boyle* [1992, 1995]). It seems consistent, however, with records of benthic Cd/Ca and Ba/Ca from Southern Ocean deposits, suggesting relatively minor glacial-interglacial changes in NADW flux to this basin [*Boyle*, 1992; *Lea*, 1995; *Rosenthal et al.*, 1997]. Clearly, the apparent discordance between different paleoceanographic proxies must be solved in order to understand the role of the THC during the transition between the two largest climatic extrema of the last 21 kyr.

In this paper we explore the sensitivity of $^{231}Pa/^{230}Th$ of Atlantic and Southern Ocean sediments to changes in the THC. We embed a simple description of trace metal scavenging into a circulation-biogeochemistry ocean model (section 2). The model is calibrated using water column data and Holocene sediment data of A_{Pa-231} and A_{Th-230} representative of the open ocean (section 3). We then examine the influence of the THC on the sediment $^{231}Pa/^{230}Th$ ratio (section 4) and discuss the paleoceanographic implications of our model results (section 5).

2. Model Description

The activities of dissolved and particulate ^{231}Pa and ^{230}Th increase generally with depth in the open ocean [*Nozaki et al.*, 1987; *Luo et al.*, 1995; *Roy-Barman et al.*, 1996; *Moran et al.*, 1997; *Rutgers van der Loeff and Berger*, 1993; *Walter et al.*, 1997]. This implies that for both metals the exchange between the dissolved and particulate phase must be reversible and occur continuously as the particles sink to the seafloor [*Bacon and Anderson*, 1982]. According to the reversible exchange model [*Nozaki et al.*, 1981; *Bacon and Anderson*, 1982], a particle-reactive metal is adsorbed onto and desorbed from settling particles assuming first-order kinetics for both processes. The continuity equations for the metal activity in dissolved form (A_d) and particulate form (A_p) read

$$\frac{\partial A_d}{\partial t} = T(A_d) + \beta + (k_{-1}A_p) - [(k_1 + \lambda)A_d] \quad (1)$$

$$\frac{\partial A_p}{\partial t} = T(A_p) - S\frac{\partial A_p}{\partial z} + (k_1 A_d) - [(k_{-1} + \lambda)A_p], \quad (2)$$

where t is time, z is depth, T is the transport by fluid advection, eddy diffusion, and convection, β is the radioactive ingrowth from U decay, k_1 and k_{-1} are the rate constants for adsorption and desorption, respectively, and S is an average particle sinking velocity.

We embed (1) and (2) into a zonally averaged, circulation-biogeochemistry ocean model [*Marchal et al.*, 1998]. The circulation component of this model is the global ocean circulation model of *Wright and Stocker* [1992], which provides the transport of ^{231}Pa and ^{230}Th in dissolved and particulate forms ($T(A_d)$ and $T(A_p)$; the sedimentation term $S\partial A_p/\partial z$ is discretized using the same scheme as for advection but without the correction for numerical diffusion). The Atlantic, Indian, and Pacific are represented as individual flat bottom basins (water depth of 4 km) and connected by a well-mixed Southern Ocean (for model grid, see *Stocker and Wright* [1996]). The circulation parameters adopted here produce a satisfactory fit to the basin mean vertical profiles of temperature, salinity, and ^{14}C activity of dissolved inorganic carbon (DIC) observed in the modern ocean [*Marchal et al.*, 1998, Table 1]. The biogeochemistry model component, on the other hand, accounts for the effect of the quantity and quality of the sinking particles on ^{231}Pa and ^{230}Th scavenging. This component includes a description of the cycles of organic carbon

and carbonate particles [*Marchal et al.*, 1998]. The biogeochemical parameters lead to a reasonable agreement with the distribution of PO_4, apparent O_2 utilization, DIC, alkalinity, and $^{13}C/^{12}C$ ratio of DIC observed in the modern ocean [*Marchal et al.*, 1998, Table 2].

2.1. Scavenging Intensities

Our description of scavenging must include the factors potentially responsible for the ^{231}Pa deficit in Atlantic sediments and ^{231}Pa excess in Southern Ocean sediments. Whereas the low Atlantic $^{231}Pa/^{230}Th$ is likely due to preferential southward export of ^{231}Pa by the NADW [*Yu et al.*, 1996], two different factors could contribute to the $^{231}Pa/^{230}Th > 0.093$ in the Southern Ocean. First, ^{231}Pa originating from the Atlantic could be scavenged in the Southern Ocean owing to the large vertical particle fluxes associated with the productive polar fronts [*Kumar et al.*, 1993; *Yu et al.*, 1996; *Boyle*, 1996]. Second, the lower fractionation factor f in the Southern Ocean resulting from the presence of biogenic opal [*Rutgers van der Loeff and Berger*, 1993; *Walter et al.*, 1997] could contribute to the efficient removal of ^{231}Pa in this basin.

In order to represent these factors in our model the adsorption rate constants k_1^{Pa} and k_1^{Th} are scaled according to the vertical flux of particulate organic matter F_{pom}, carbonate particles F_{car}, and opal F_{opal} at the base of the euphotic zone (100 m):

$$k_1^{Pa} = \left(\sigma_{pom}^{Pa} F_{pom}\right) + \left(\sigma_{car}^{Pa} F_{car}\right) + \left(\sigma_{opal}^{Pa} F_{opal}\right) \quad (3)$$

$$k_1^{Th} = \left(\sigma_{pom}^{Th} F_{pom}\right) + \left(\sigma_{car}^{Th} F_{car}\right) + \left(\sigma_{opal}^{Th} F_{opal}\right). \quad (4)$$

These expressions are explicit statements of the classical view that the removal of particle-reactive metals from the water column depends on the amount of particles produced in the surface layers, although a linear dependence is not necessarily postulated [*Bacon*, 1988]. We assume that the scaling factors σ ($m^2\ mol^{-1}$) are spatially uniform, so that k_1^{Pa} and k_1^{Th} vary with latitude and basin but not with depth. Depth-invariant k_1^{Pa} and k_1^{Th} lead to simulations of linear vertical profiles of dissolved and particulate A_{Th-230} and A_{Pa-231} if deep water transport is not significant [*Bacon and Anderson*, 1982]. This prediction is consistent with precise water column measurements, e.g., in the central North Pacific [*Roy-Barman et al.*, 1996].

We make two remarks regarding our description of scavenging. First, (3) and (4) neglect the possible role of lithogenic particles, considering that the vertical flux of particles in the open ocean (which dictates the sediment $^{231}Pa/^{230}Th$) is chiefly biogenic [*Honjo*, 1980; *Honjo et al.*, 1982]. *Luo and Ku* [1999] presented a negative correlation between $^{231}Pa/^{230}Th$ and ^{232}Th concentration for sediment trap and sediment materials from the equatorial Pacific and Blake Outer Ridge (North Atlantic). These authors interpreted the correlation as reflecting a strong preference by clay particles for Th and then speculated that these particles could be important in Th–Pa fractionation in ocean waters. Whereas the importance of clays remains speculative, their possible contribution should be included in Th–Pa scavenging models if it is proved significant. Second, our description of scavenging is different from the one used to simulate ^{230}Th in a three-dimensional, circulation-biogeochemistry ocean model [*Henderson et al.*, 1999]. In the latter model the ^{230}Th partitioning between the dissolved and particulate phase is related indirectly to surface particle production through a particle concentration-dependent distribution coefficient $K_d = A_p/(A_d C_p)$, where C_p is the local concentration of particulate organic matter, carbonate particles, or opal. We do not follow this approach here, for the possible effect of C_p on K_d is not known for Pa.

2.2. Affinity Factors

The scaling factors σ ($m^2\ mol^{-1}$) in (3) and (4) depict the affinity of each biogenic phase for Th and Pa. We are not aware of experimental data which document the relative preference of each biogenic phase for Th. We follow therefore *Henderson et al.* [1999] by assuming that Th is equally reactive for each phase. Likewise, there seems to be no experimental data to support a different affinity of particulate organic matter and carbonate particles for Pa. By contrast, determinations of the fractionation factor in the field [*Walter et al.*, 1997] and in the laboratory [*Anderson et al.*, 1992] indicate that particulate silica fractionates Pa and Th much less strongly than other marine particles. We thus assume

$$\sigma_{pom}^{Th} = \sigma_{car}^{Th} = \sigma_{opal}^{Th} = \sigma^{Th}, \quad (5)$$

$$\sigma_{pom}^{Pa} = \sigma_{car}^{Pa} = \frac{\sigma^{Th}}{f_{pom,car}}, \quad (6)$$

$$\sigma_{opal}^{Pa} = \frac{\sigma^{Th}}{f_{opal}}, \quad (7)$$

where $f_{pom,car}$ and f_{opal} are fractionation factors. Determinations of the fractionation factor in oceanic environments where biogenic silica is not produced in large amounts [*Nozaki and Nakanishi*, 1985; *Walter et al.*, 1997] suggest that $f_{pom,car} \sim 10$. On the other hand, the factors measured in Southern Ocean waters [*Rutgers van der Loeff and Berger*, 1993; *Walter et al.*, 1997] and on a suspension of silica gel [*Anderson et al.*, 1992] suggest that $f_{opal} \sim 1$.

2.3. Particle Fluxes

The vertical fluxes F_{pom}, F_{car}, and F_{opal} are provided by the biogeochemistry model component. F_{pom} de-

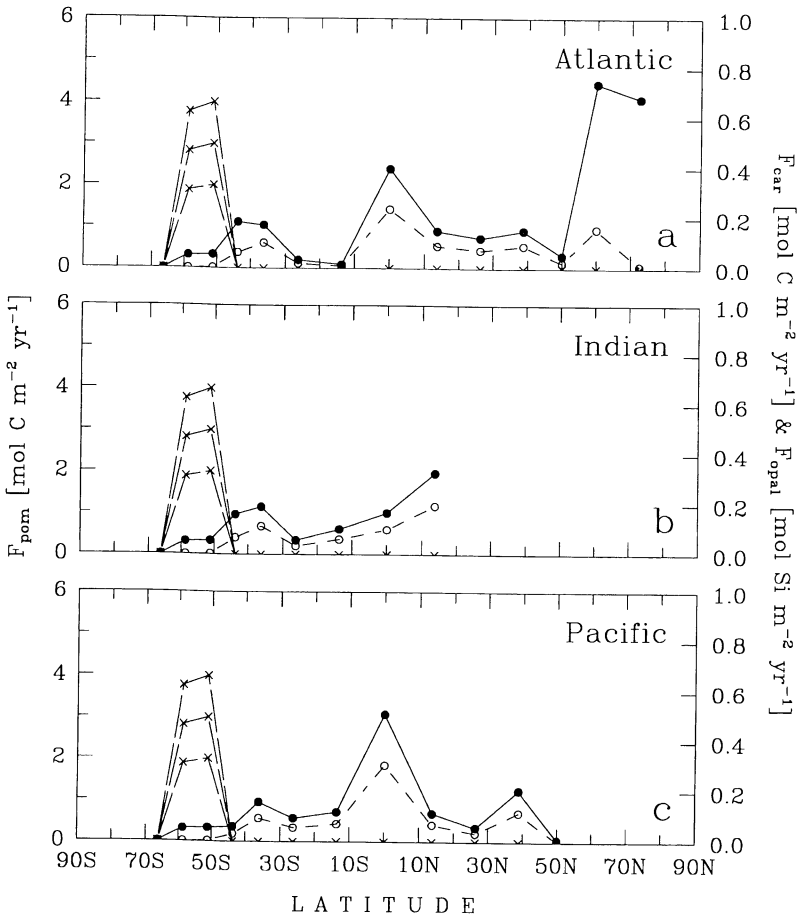

Figure 1. Latitudinal profiles of the vertical flux of particulate organic matter (solid circles), carbonate particles (open circles), and opal (crosses) at the base of the euphotic zone (100 m) predicted by the zonally averaged model for modern circulation conditions. Opal fluxes calculated with a production ratio of 1.0 mol Si (mol C)$^{-1}$ (reference simulation), 1.5 mol Si (mol C)$^{-1}$, and 2.0 mol Si (mol C)$^{-1}$ are shown. Note that the scale is different for F_{pom} (left scale) and for F_{car} and F_{opal} (right scale).

pends on the availability of phosphate (taken as the limiting nutrient) in the euphotic zone, whereas F_{car} depends on both PO_4 and temperature [*Marchal et al.*, 1998]. F_{pom} and F_{car} simulated for modern circulation conditions (with 24 Sv of waters formed in the North Atlantic; 1 Sv = 10^6 m^3 s^{-1}) exhibit maxima in the northern North Atlantic, at subpolar latitudes, and in equatorial regions of Ekman divergence (solid and open circles in Figures 1a–1c).

We need, on the other hand, to represent the export flux of opal in the Southern Ocean [e.g., *Walter et al.*, 1997]. The large-scale production of opal in this basin is usually estimated by scaling with measurements of primary productivity [*Spencer*, 1983; *Nelson et al.*, 1995]. This approach considers that diatoms (siliceous phytoplankton) are a major producer of both new organic carbon and particulate silica in Antarctic waters. We adopt a similar approach by relating F_{opal} to F_{pom} in the model:

$$F_{opal} = rF_{pom}, \quad (8)$$

where r is a production ratio (mol Si (mol C)$^{-1}$). We constrain r so as to simulate a net rate of opal production in the Southern Ocean consistent with available observational estimates. The gross rate of opal production in this basin was estimated at 17–37 Tmol Si yr^{-1} [*Nelson et al.*, 1995]. To infer the net rate, we need to account for the dissolution of opaline particles in the upper water column [*Wollast*, 1974; *Spencer*, 1983]. *Nelson and Gordon* [1982] estimated a silica dissolution/production ratio of 0.18–0.58 in the Antarctic circumpolar current. We hence infer an estimate of net opal production in the Southern Ocean of 3.1–21 Tmol Si yr^{-1}. We use r = 1 mol Si (mol C)$^{-1}$ as a reference value in our model. This yields a net opal production integrated over the Southern Ocean area of 13 Tmol Si yr^{-1}, in the middle of the range of observational estimates. We note that F_{opal} is nil at the southernmost grid cell of the Southern Ocean (crosses in Figure 1c) owing to insufficient deep water PO_4 supply simulated at this location [*Marchal et al.*, 1998].

Table 1. Water Column ^{230}Th Data Used in This Study[a]

Reference	Ocean Basin	Dissolved	Particulate	Total
Krishnaswami et al. [1976]	South, tropical, and North Pacific		Y	
Nozaki et al. [1981]	North Pacific			Y
Moore [1981]	tropical Pacific	Y		
Anderson et al. [1983a]	tropical Pacific and North Atlantic	Y		
Nozaki and Horibe [1983]	North Pacific	Y		
Nozaki and Nakanishi [1985]	tropical and North Pacific			Y
Nozaki et al. [1987]	North Pacific	Y	Y	Y
Rutgers van der Loeff and Berger [1993]	South Atlantic	Y	Y	Y
Luo et al. [1995]	tropical Pacific			Y
Colley et al. [1995]	North Atlantic	Y	Y	Y
Roy-Barman et al. [1996]	tropical Pacific	Y		Y
Moran et al. [1997]	North Atlantic	Y	Y	Y
Walter et al. [1997]	South Atlantic	Y	Y	Y
Vogler et al. [1998]	North Atlantic	Y	Y	Y
R. François (unpublished data, 1999)	South and tropical Atlantic	Y		Y

[a]All ^{230}Th activities are expressed in dpm m^{-3} (disintegrations per minute per cubic meter of water), assuming a seawater density of 1028 kg m^{-3} and using the conversion 1 fg $^{230}Th \equiv 4.48 \times 10^{-5}$ dpm. Y, yes.

Whereas opal production outside the Southern Ocean is neglected, this production does not alter the Atlantic and Southern Ocean $^{231}Pa/^{230}Th$ in our model (section 5).

In summary, the simulation of ^{231}Pa and ^{230}Th requires six additional parameters: σ^{Th}, $f_{pom,car}$, f_{opal}, r, k_{-1} (taken the same for both metals), and S. We examine the sensitivity of the sediment $^{231}Pa/^{230}Th$ ratio to each parameter in section 3.2.

2.4. Global Radiochemical Balance

The world ocean balance for ^{231}Pa and ^{230}Th is achieved in the model when the net radioactive production of dissolved ^{231}Pa and ^{230}Th in the water column equals the sedimentation flux of the two isotopes at the ocean bottom (depth z_b):

$$\int [\beta - \lambda (A_d + A_p)] \, dv = \int - (SA_p)\,|_{z_b} ds, \quad (9)$$

where the integrations are over the whole ocean volume v and surface area s. The model is integrated for 10,000 years, sufficient to produce a quasi-steady state distribution for each tracer. The "sediment" $^{231}Pa/^{230}Th$ in the model is the $^{231}Pa/^{230}Th$ of particles in the deepest grid cell (3.5–4 km).

3. Simulation of ^{231}Pa and ^{230}Th in Holocene Ocean

We have selected from the literature water column and Holocene sediment data of ^{231}Pa and ^{230}Th, presumably representative of the open ocean (Tables 1–3). Although differences in analytical techniques between different studies likely contribute to the variability in the selected data set, the data suggest some robust features in the large-scale distribution of ^{231}Pa and ^{230}Th, as discussed below.

3.1. Results for Water Column

The observed activities of dissolved and particulate ^{230}Th (and hence of total ^{230}Th) are generally lower in the northern North Atlantic (north of 45°N) than in the Southern Ocean (south of 47°S) and the North Pa-

Table 2. Water Column ^{231}Pa Data Used in This Study[a]

Reference	Ocean Basin	Dissolved	Particulate	Total
Anderson et al. [1983a]	tropical Pacific and North Atlantic	Y		
Nozaki and Nakanishi [1985]	tropical Pacific			Y
Rutgers van der Loeff and Berger [1993]	South Atlantic	Y	Y	Y
Walter et al. [1997]	South Atlantic	Y	Y	Y
R. François (unpublished data, 1999)	tropical Atlantic	Y		

[a]All ^{231}Pa activities are expressed in dpm m^{-3}, assuming a seawater density of 1028 kg m^{-3}. Y, yes.

Table 3. Data of Holocene Sediment $^{231}Pa/^{230}Th$ Ratio Used in This Study

Reference	Ocean Basin
Ku [1966]	North Atlantic and South Pacific
Ku et al. [1972]	North Atlantic
DeMaster [1979]	South Atlantic
Bacon and Rosholt [1982]	South Atlantic
Mangini and Dieter-Haass [1983]	North Atlantic
Anderson et al. [1983a]	North Atlantic
Yang et al. [1986]	South Pacific
Lao et al. [1992]	South Pacific
Anderson et al. [1994]	North Atlantic
Legeleux [1994]	North Atlantic
Kumar [1994]	South Atlantic
Yu [1994]	South and North Atlantic
Scholten et al. [1995]	North Atlantic
Walter et al. [1997]	South Atlantic
Asmus et al. [1999]	South Atlantic
H. Walter (unpublished data, 1999)	South Pacific

cific (Figures 2a–2c). The low activities in the northern North Atlantic were ascribed to the injection to depth of ^{230}Th-poor NADW [*Moran et al.*, 1997; *Vogler et al.*, 1998]. On the other hand, the upwelling of ^{230}Th-rich, lower Circumpolar Deep Water is presumably responsible for the high activities south of the Antarctic polar front ($\sim 50°S$; *Rutgers van der Loeff and Berger* [1993]). The available data suggest that the activity gradient between the Atlantic and the Southern Ocean is lower for dissolved ^{231}Pa than for dissolved ^{230}Th (compare Figure 3a with Figure 2a).

Water column A_{Pa-231} and A_{Th-230} data are compared with model results for modern circulation conditions. We use estimates of the scavenging parameters $f_{pom,car}$, f_{opal}, r, k_{-1}, and S from the literature and then determine σ^{Th} so as to obtain a reasonable agreement with these data. We take the following values: $f_{pom,car} = 10$ [*Nozaki and Nakanishi*, 1985; *Walter et al.*, 1997]; $f_{opal} = 1$ [*Rutgers van der Loeff and Berger*, 1993; *Walter et al.*, 1997; *Anderson et al.*, 1992]; $r = 1.0$ mol Si (mol C)$^{-1}$ (section 2.3); $k_{-1} = 3$ yr^{-1}, the average of estimates by *Bacon and Anderson* [1982] based on vertical profiles of dissolved and particulate A_{Th-230}; and $S = 700$ m yr^{-1}, in the range of estimates of 3×10^2 to 9×10^2 m yr^{-1} from vertical profiles of particulate A_{Th-230} in various ocean settings [*Krishnaswami et al.*, 1976, 1981; *Rutgers van der Loeff and Berger*, 1993; *Scholten et al.*, 1995].

A reasonable agreement with data of both A_{Th-230} and A_{Pa-231} is obtained with σ^{Th} in the range 0.375–1.125 m^2 mol^{-1} (Figures 2 and 3). The model replicates the low activities of dissolved and particulate A_{Th-230} in the northern North Atlantic and the high activities in the Southern Ocean and North Pacific (Figures 2a–2b). The simulated southward increase in A_{Th-230} from the northern North Atlantic to the Southern Ocean is related to scavenging and deep ocean ventilation, both being relatively high in the former region and low in the latter region. The difference in scavenging intensity between the two regions stems from the different amplitude in the vertical flux of biogenic particles (Figure 1a). The difference in deep ventilation, on the other hand, is illustrated by the ^{14}C activity of DIC, which is high in the northern North Atlantic and low in the Southern Ocean in the simulation of modern circulation conditions [*Marchal et al.*, 1999, Figure 7a]. The model also predicts ^{231}Pa activities and partitioning between the dissolved and particulate phase, which are broadly consistent with the available data (Figure 3).

3.2. Results for Sediments

Data of the $^{231}Pa/^{230}Th$ ratio in Holocene sediments reveal clearly the ^{231}Pa deficit in the Atlantic and ^{231}Pa excess in the Southern Ocean (circles in Figure 4a). Note that the data for the Southern Ocean come to a large extent from the Atlantic sector of this basin [*Walter et al.*, 1997]. The $^{231}Pa/^{230}Th$ ratio at the margins in the Atlantic basin barely exceeds the production ratio of 0.093 [*Yu et al.*, 1996]. This indicates that the preferential deposition of ^{231}Pa at the margins (boundary scavenging) is weak in the Atlantic [*Yu et al.*, 1996], in contrast to the Pacific [*Lao et al.*, 1992; *Walter et al.*, 1999]. This suggests that using a zonally averaged model (which cannot represent boundary scavenging) is a reasonable first-order approach to simulate the behavior of ^{231}Pa and ^{230}Th in the Atlantic and Southern Ocean.

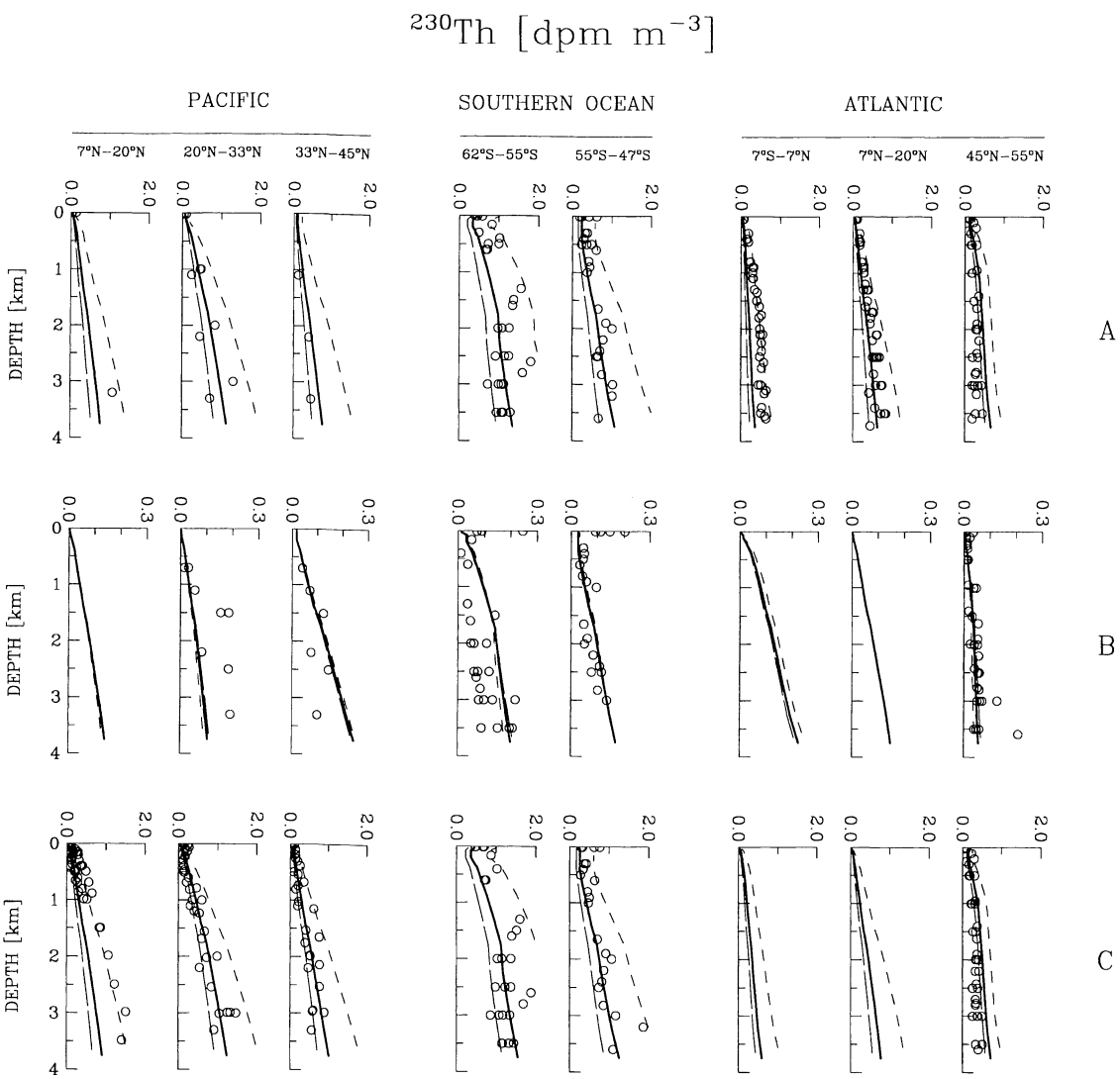

Figure 2. Vertical profiles of (a) dissolved ^{230}Th, (b) particulate ^{230}Th, and (c) total ^{230}Th in the ocean water column. The open circles are measurements (for references, see Table 1). The curves are model results for modern circulation conditions with a scavenging affinity $\sigma^{Th} = 0.375$ m^2 mol^{-1} (short-dashed curve), 0.750 m^2 mol^{-1} (solid curve), and 1.125 m^2 mol^{-1} (long-dashed curve). The values of the other scavenging parameters are reported in Table 4.

The observed pattern of ^{231}Pa depletion in the Atlantic and ^{231}Pa enrichment in the Southern Ocean can indeed be reasonably reproduced by the zonally averaged model (solid curve in Figures 4a–4e). Sensitivity tests demonstrate that this pattern persists if the scavenging parameters σ^{Th}, $f_{pom,car}$, r, k_{-1}, and S are changed individually by ±50% (Figures 4a–4e). Interestingly, the high $^{231}Pa/^{230}Th$ observed in the Southern Ocean cannot be replicated with $f_{opal} = f_{pom,car} = 10$ (dashed curve with pluses in Figure 4b). This confirms that less fractionation between the two metals by opal would be a major contributor to the excess ^{231}Pa activities observed in Holocene sediments of the Southern Ocean [e.g., *Walter et al.*, 1997]. Opal would thus be an important factor that transforms the Southern Ocean into a ^{231}Pa sink. Without opal and its relatively high affinity for Pa, the THC would export ^{231}Pa from the Atlantic into the Indian and Pacific.

In our reference simulation (solid curve in Figures 2–4; for model parameters, see Table 4) the fractions of ^{231}Pa and ^{230}Th produced in the Atlantic (47°S–80°N) and exported to the Southern Ocean reach 0.27 and 0.02, respectively. These values are lower than the observational estimates ($\sim$ 0.45 for ^{231}Pa and $\sim$ 0.15 for ^{230}Th [*Yu et al.*, 1996]). On the one hand, we may underestimate the export of the two radionuclides to the Southern Ocean owing, e.g., to a too high scavenging intensity in the equatorial Atlantic (Figure 2a and

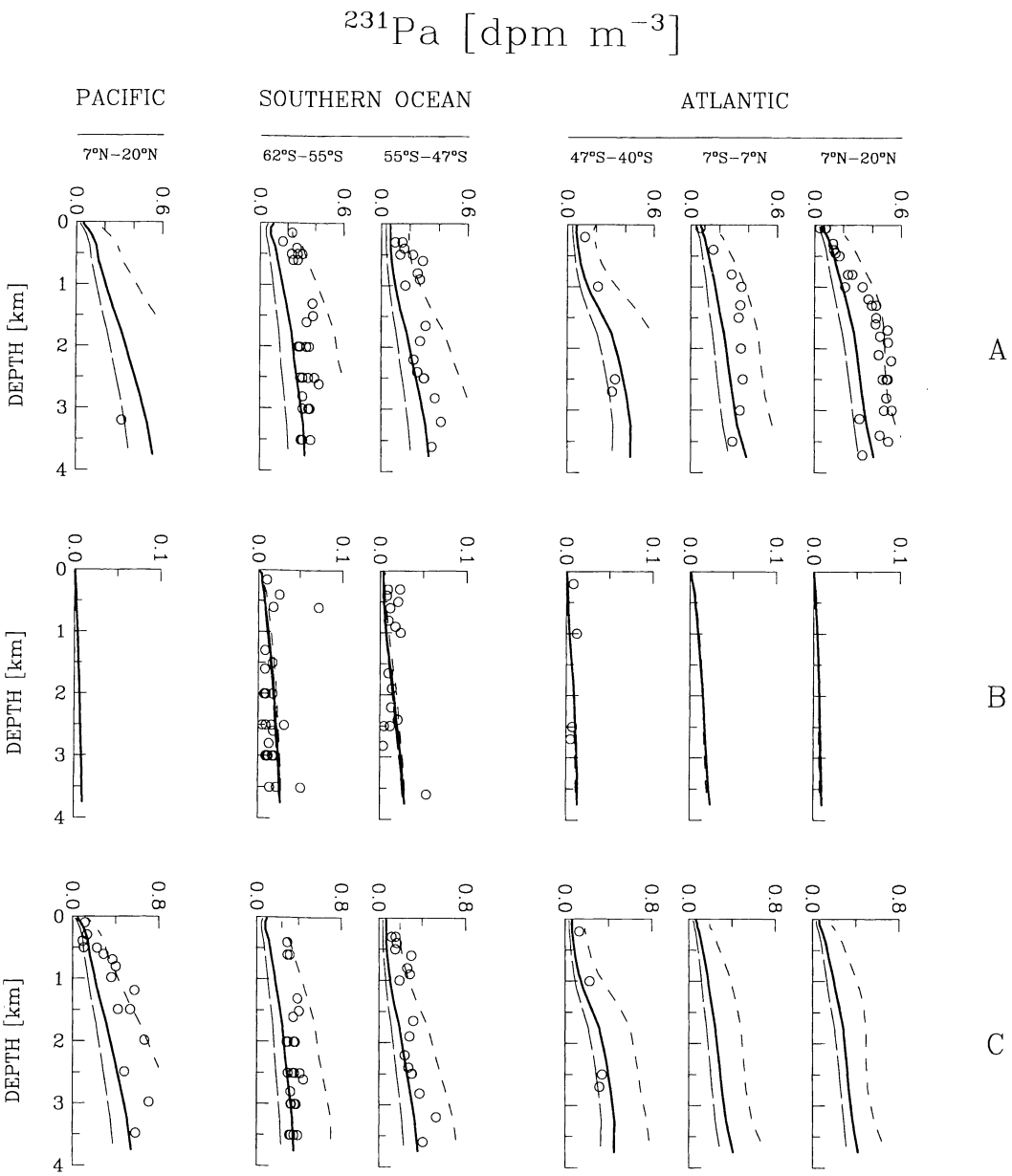

Figure 3. Vertical profiles of (a) dissolved ^{231}Pa, (b) particulate ^{231}Pa, and (c) total ^{231}Pa in the ocean water column. The open circles are measurements (for references, see Table 2). The curves are model results for modern circulation conditions with the scavenging affinities σ^{Pa}_{pom}, σ^{Pa}_{car}, and σ^{Pa}_{opal} calculated with $\sigma^{Th} = 0.375$ m^2 mol^{-1} (short-dashed curve), 0.750 m^2 mol^{-1} (solid curve), and 1.125 m^2 mol^{-1} (long-dashed curve) (see (6) and (7) in the text). The values of the other scavenging parameters are reported in Table 4.

Figure 4a). On the other hand, the observational estimates reported by *Yu et al.* [1996] are based on very limited water column data and still need corroboration. We note that the ratio between ^{231}Pa flux at the ocean bottom and depth-integrated ^{231}Pa production in the water column averages 0.73 in the Atlantic and 1.58 in the Southern Ocean. The ratio for ^{230}Th averages 0.98 in the Atlantic and 0.94 in the Southern Ocean. Thus the high $^{231}Pa/^{230}Th$ simulated in the Southern Ocean are due largely to enhanced ^{231}Pa scavenging in this basin, owing to the production of biogenic opal [see also *Rutgers van der Loeff and Berger*, 1993; *Walter et al.*, 1997].

4. Sensitivity to Deep-Ocean Circulation

We consider a sample of simulations characterized by different THC strengths and the same values of the scavenging parameters (Table 4), as determined previ-

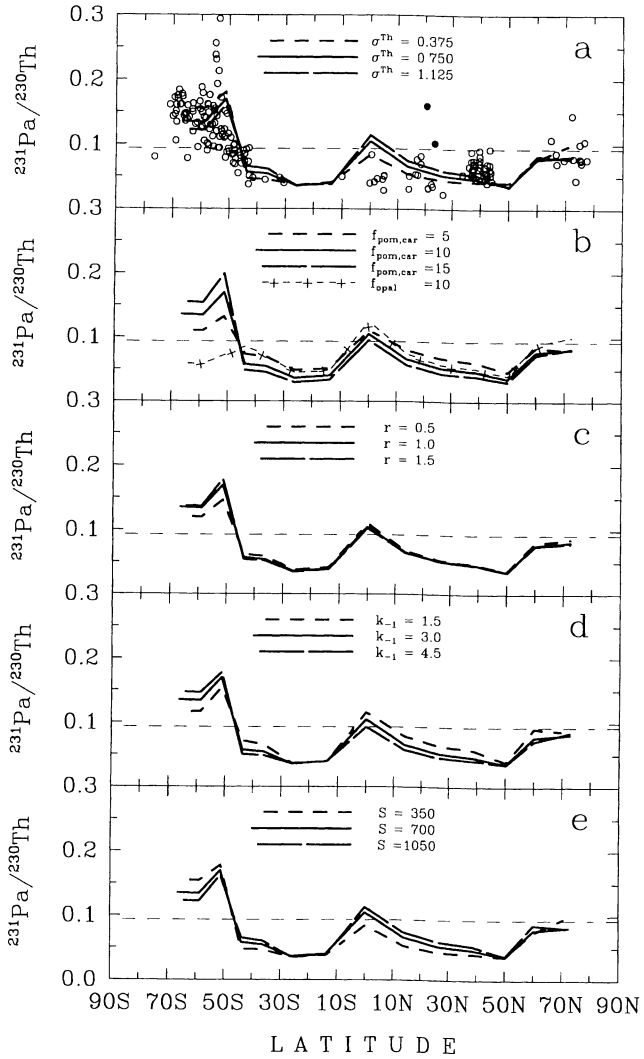

Figure 4. Latitudinal profiles of the sediment $^{231}Pa/^{230}Th$ in the Atlantic and Southern Ocean. The circles in Figure 4a are measurements in Holocene (0–10 kyr B.P.) sediments (for references, see Table 3); two high $^{231}Pa/^{230}Th$ values (from off West Africa), reflecting presumably boundary scavenging, are shown as solid circles. The curves correspond to model results for modern circulation conditions with (a) $\sigma^{Th} = 0.375$ m^2 mol^{-1} (short-dashed curve), 0.750 m^2 mol^{-1} (solid curve), and 1.125 m^2 mol^{-1} (long-dashed curve); (b) $f_{pom,car} = 5$ (short-dashed curve), 10 (solid curve), 15 (long-dashed curve), and $f_{opal} = 10$ (plus dashed curve); (c) $r = 0.5$ mol Si (mol C)$^{-1}$ (short-dashed curve), 1.0 mol Si (mol C)$^{-1}$ (solid curve), and 1.5 mol Si (mol C)$^{-1}$ (long-dashed curve); (d) $k_{-1} = 1.5$ yr^{-1} (short-dashed curve), 3.0 yr^{-1} (solid curve), and 4.5 yr^{-1} (long-dashed curve); and (e) $S = 350$ m yr^{-1} (short-dashed curve), 700 m yr^{-1} (solid curve), and 1050 m yr^{-1} (long-dashed curve). The values of the other scavenging parameters in Figures 4a–4e are reported in Table 4. The horizontal dashed line in each panel denotes the production ratio of the two radionuclides in the ocean water column.

ously (section 3). The different THC strengths were generated by changing the restoring value of surface salinity at the northernmost grid cell in the Atlantic, S_{NA} [*England*, 1992; *Stocker et al.*, 1992]. We use a three-step procedure for each simulation. In step 1 the model is integrated for 10,000 years to a first steady state using a S_{NA} representative of newly formed deep waters in the modern North Atlantic. This state corresponds to the reference simulation considered in section 3. The production of organic matter in the euphotic zone is calculated from a restoring to climatological PO_4 data [*Marchal et al.*, 1998]. In order to account for the effect of circulation changes on the biogenic fluxes F_{pom}, F_{car}, and F_{opal} we replace in step 2 the restoring approach by a prognostic approach, where this production is described as a function of local PO_4 using Michaelis-Menten kinetics [*Marchal et al.*, 1999]. The tracer distributions remain virtually unaltered from step 1 to step 2. Finally, in step 3 the model is integrated for an additional 10,000 years using a different S_{NA}.

4.1. Changes in Latitude Distribution of $^{231}Pa/^{230}Th$

The $^{231}Pa/^{230}Th$ generally increases north of $\sim 30°S$ in the Atlantic and decreases south of this latitude, when the THC strength is reduced from 24 to 3 Sv (compare thick solid curve with thin solid curve in right panel of Figures 5b–5e). The predicted $^{231}Pa/^{230}Th$ changes are due to the direct effect of the THC on the transport of the two metals as well as to its indirect effect through varying scavenging intensities (k_1^{Pa} and k_1^{Th}, both depending on the biogenic particle fluxes through (3) and (4) and hence on the circulation-driven deep water supply of PO_4). To elucidate the direct effect, we consider a series of simulations where k_1^{Pa} and k_1^{Th} are kept fixed to their values of the reference simulation. We find almost the same results as with variable scavenging intensities (compare dashed curve with thin solid curve in right panel of Figures 5b–5e).

The fraction of ^{231}Pa produced in the Atlantic and exported to the Southern Ocean decreases from 0.27 to 0.08 when the THC drops from 24 Sv (left panel of Figure 5a) to 3 Sv (Figure 5e). The fraction for ^{230}Th is ≤ 0.02 in all the simulations, indicating that almost all the ^{230}Th produced in the Atlantic remains there. We thus ascribe the $^{231}Pa/^{230}Th$ rise simulated in the North Atlantic to a longer residence time of ^{231}Pa in this basin when THC is reduced, permitting more efficient scavenging. Likewise, the $^{231}Pa/^{230}Th$ decrease in the Southern Ocean is due to smaller ^{231}Pa import from the Atlantic. We note that $^{231}Pa/^{230}Th$ in the northernmost Atlantic when the THC is completely shut down is smaller than in the reference simulation (right panel of Figure 5e). The biogenic particle fluxes in this region decrease drastically owing to reduced convective activity and deep water supply of PO_4 (middle panel of Figure 5e). The effect on $^{231}Pa/^{230}Th$ of the resulting decrease in scavenging intensity exceeds the ventilation effect.

Table 4. Parameters of the Scavenging Model

Parameter	Description	Value
σ^{Th}	efficiency of Th scavenging	0.75 m^2 mol^{-1}
$f_{pom,car}$	Th–Pa fractionation factor[a]	10
f_{opal}	Th–Pa fractionation factor[b]	1
r	production ratio in Southern Ocean[c]	1.0 mol Si (mol C)$^{-1}$
k_{-1}	desorption rate constant for Pa and Th	3.0 $year^{-1}$
S	average particle sinking velocity	700 m yr^{-1}

[a]For particulate organic matter and carbonate particles
[b]For biogenic silica
[c]Between biogenic silica and particulate organic matter

4.2. Changes in Basin Mean $^{231}Pa/^{230}Th$

From the similarity between their estimates of the Atlantic mean $^{231}Pa/^{230}Th$ of the Holocene and LGM, *Yu et al.* [1996] argued that the THC did not vary significantly between the two climatic periods. Here we attempt to provide a more quantitative estimate of the change in THC between these two periods by comparing the mean $^{231}Pa/^{230}Th$ calculated from the updated database with model-predicted changes.

The geographic distribution of the current database [*Walter et al.*, 1999] is still too limited to make a rigorous estimate of the mean $^{231}Pa/^{230}Th$ of Atlantic sediments. As mentioned previously, however, boundary scavenging in the Atlantic is minimal, presumably due to the comparatively short residence time of the deep waters in this basin. It can thus be anticipated that the environmentally controlled geographic variability of $^{231}Pa/^{230}Th$ is small and that much of the variability present in the current database (e.g., right panel of Figure 5a) is due to analytical or stratigraphic errors that are distributed randomly. If so, the Atlantic mean $^{231}Pa/^{230}Th$ and its uncertainty can be estimated from the mean and variance of all the values from the database. We note that this approach cannot be applied to the Southern Ocean because of the large and systematic variation of $^{231}Pa/^{230}Th$ across the polar frontal zone (Figure 5a). To accommodate this variability, we would need a synoptic data set over the entire region. While the Atlantic sector is fairly well covered [*Walter et al.*, 1997, 1999], the data available from the remainder of the Southern Ocean are too sparse.

We find that the mean $^{231}Pa/^{230}Th$ of Holocene Atlantic sediments (north of 45°S) equals 0.065±0.005 (n = 90; Table 5). The uncertainty of 0.005 is half the 95% confidence interval calculated for one normal mean with unknown variance [*Dudewicz and Mishra*, 1988; p. 555]. Two samples from the upwelling region off West Africa seem influenced by boundary scavenging (solid circles in Figure 5a). Removing them from the database, however, does not change the mean and variance significantly (0.063±0.004; n = 88). *Yu et al.* [1996] found similar results, using a subset of the present database (0.060±0.004; n = 68).

Calculating the Atlantic mean $^{231}Pa/^{230}Th$ for the LGM is more delicate, as boundary scavenging off West Africa appears to have been more pronounced [*Yu et al.*, 1996]. If we neglect this effect and consider that our entire database is normally distributed, we find that the mean $^{231}Pa/^{230}Th$ of the glacial Atlantic (north of 45°S) is 0.063±0.011 (n = 29; Table 5). If we remove the three cores off West Africa with a $^{231}Pa/^{230}Th \geq 0.12$, we find 0.054±0.006 ($n$ = 26). In the first approach we probably overestimate the mean and variance, while we underestimate them in the second approach. To address this problem, *Yu et al.* [1996] assumed that the upwelling region off West Africa occupied 3% of the whole Atlantic surface area and calculated an area-weighted average of the glacial Atlantic $^{231}Pa/^{230}Th$ of 0.059±0.007 (n = 29). However, because of the lack of synoptic data, it is difficult to estimate the errors on the surface area and the $^{231}Pa/^{230}Th$ of the upwelling region. We thus use the two previous estimates to bracket the mean and variance of the glacial Atlantic $^{231}Pa/^{230}Th$.

The difference between the Atlantic mean $^{231}Pa/^{230}Th$ of the LGM and Holocene, Δ_A, is –0.002 if data from off West Africa are included and –0.009 if these data are removed. We estimate the uncertainty in this difference from the 95% confidence interval (CI) for the difference between two normal means in case where the population variances are unknown but equal. The length of the CI (twice the uncertainty) is calculated as [*Dudewicz and Mishra*, 1988]

$$CI = 2t_{n_1+n_2-2}\sqrt{s_p^2\left(\frac{1}{n_1}+\frac{1}{n_2}\right)}, \qquad (10)$$

where n_1 and n_2 are the numbers of $^{231}Pa/^{230}Th$ data for the LGM and Holocene, $t_{n_1+n_2-2}$ is the fractional point of the t distribution with a degree of freedom of

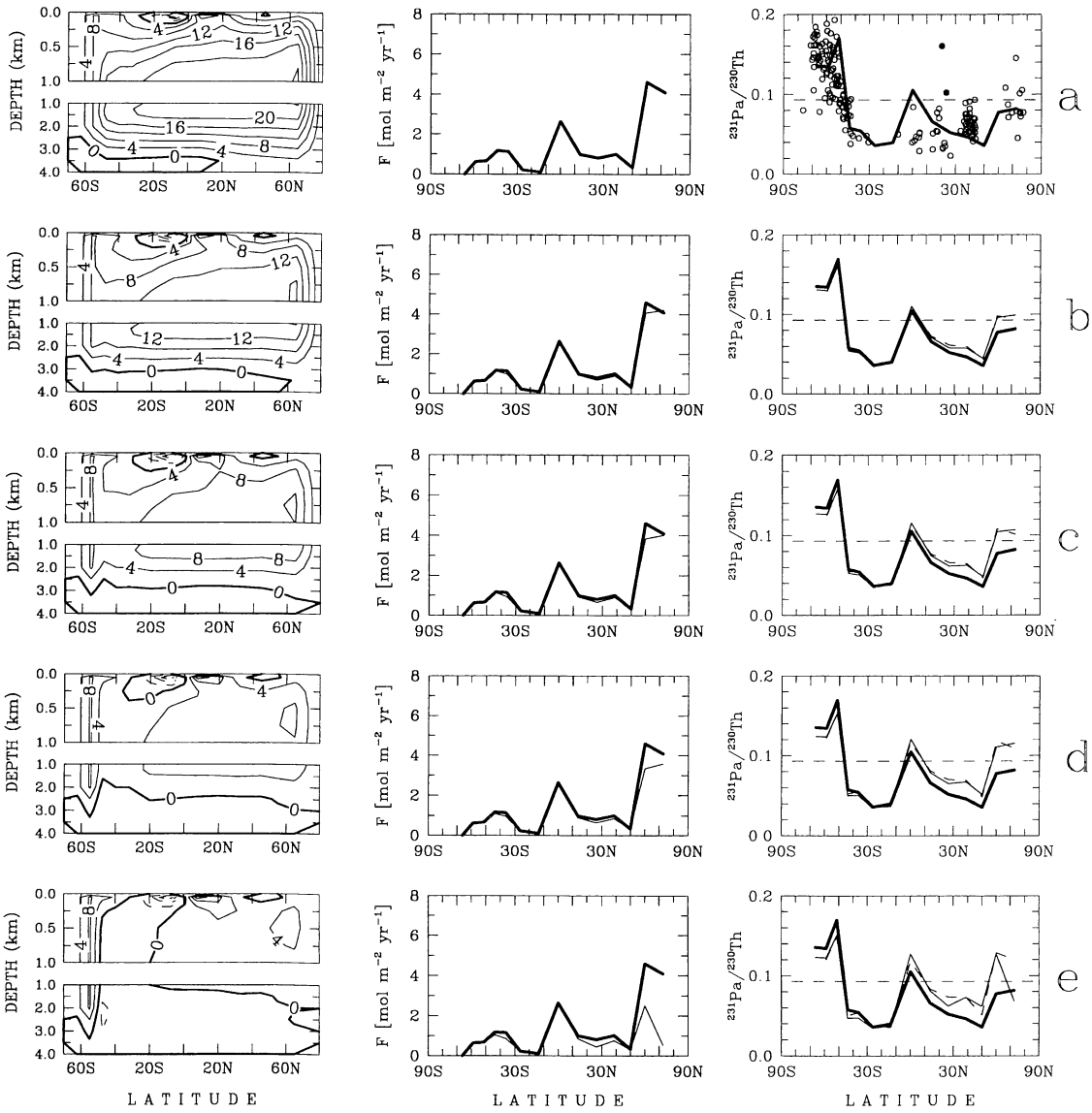

Figure 5. (left) Stream function (in Sv), (middle) total flux of biogenic particles at the base of the euphotic zone, and (right) sediment $^{231}Pa/^{230}Th$ ratio in the Atlantic and Southern Ocean in simulations where the strength of the Atlantic thermohaline circulation (THC) is (a) 24 Sv, (b) 16 Sv, (c) 12 Sv, (d) 8 Sv, and (e) 3 Sv. The total flux of biogenic particles $F = F_{pom} + F_{car} + F_{opal}$. The total particle flux and the sediment ratio predicted in the simulation with a THC strength of 24 Sv (representing presumably modern circulation conditions) are shown in each panel for reference (thick solid curve). The circles in the right panel of Figure 5a are measurements in Holocene sediments; two high $^{231}Pa/^{230}Th$ values (from off West Africa), reflecting presumably boundary scavenging, are shown as solid circles. The thin solid curve in the right panel of Figures 5b–5e displays the ratios predicted when the scavenging intensities k_1^{Pa} and k_1^{Th} are allowed to vary. The thin dashed curve in these panels shows the ratios predicted when these intensities are kept constant. The horizontal dashed line in each right panel denotes the production ratio of the two radionuclides in the ocean water column.

$(n_1 + n_2 - 2)$ at the probability level 0.975 (i.e., for a 95% confidence interval), and s_p^2 is the pooled variance,

$$s_p^2 = \frac{(n_1 - 1)s_1^2 + (n_2 - 1)s_2^2}{n_1 + n_2 - 2}, \tag{11}$$

where s_1^2 and s_2^2 are the variances of the LGM and Holocene $^{231}Pa/^{230}Th$ data. We obtain

$$\Delta_A = -0.002 \pm 0.010 \tag{12}$$

when data from off West Africa are included and

$$\Delta_A = -0.009 \pm 0.008 \tag{13}$$

when data from off West Africa are excluded. We thus conclude that at the 95% confidence level the mean

Table 5. Observational Estimates of Basin Mean $^{231}Pa/^{230}Th$ Ratios for Holocene and LGM Sediments[a]

Basin	Epoch	Mean $^{231}Pa/^{230}Th$ Data From off West Africa Included	Mean $^{231}Pa/^{230}Th$ Data From off West Africa Excluded
Atlantic[b]	Holocene	0.065±0.005 (n = 90)	0.063±0.004 (n = 88)
Atlantic[b]	LGM	0.063±0.011 (n = 29)	0.054±0.006 (n = 26)
North Atlantic[c]	Holocene	0.067±0.006 (n = 70)	0.065±0.005 (n = 68)
North Atlantic[c]	LGM	0.062±0.016 (n = 15)	0.052±0.006 (n = 13)

[a]The data used to calculate the basin averages for Holocene and LGM sediments are from the compilation of *Walter et al.* [1999] and *Yu et al.* [1996], respectively.
[b]Between 45°S and 80°N.
[c]Between 7°N and 80°N.

$^{231}Pa/^{230}Th$ of the glacial Atlantic could not have been higher by > 0.008 compared to the mean value of the Holocene Atlantic.

In our model the mean $^{231}Pa/^{230}Th$ of the entire Atlantic (47°S–80°N) rises by 0.011 (variable k_1) or 0.013 (constant k_1) for a full collapse of the THC (from 24 to 3 Sv) (Figure 6a). It rises by 0.008 (variable k_1) or 0.009 (constant k_1) for a twofold reduction in THC strength (from 24 to 12 Sv) (Figure 6a). These increases are substantially less than anticipated if the Atlantic mean $^{231}Pa/^{230}Th$ depends only on THC. In such a case, as THC approaches 0 Sv, $^{231}Pa/^{230}Th$ should approach 0.093 [*Yu et al.*, 1996, Figures 4b–4c]. In our model the poor sensitivity of the Atlantic mean $^{231}Pa/^{230}Th$ to THC strength stems from the small $^{231}Pa/^{230}Th$ changes in the South Atlantic. The South Atlantic is a hinge zone, influenced by reduced ^{231}Pa import from the north and by enhanced ^{231}Pa scavenging in the Southern Ocean where biogenic opal is produced (right panel of Figures 5a–5e). We note that $^{231}Pa/^{230}Th$ declines slightly at the southernmost grid cells in this basin in response to THC reduction (e.g., Figure 5e), even though no opal production is simulated at these locations. This decline results, at least partly, from the small decrease in bioproductivity predicted at these locations (middle panel of Figure 5e and compare thin solid curve with dashed curve in right panel of Figure 5e). We observe, finally, that $^{231}Pa/^{230}Th$ in the Southern Ocean is not very sensitive to the thermohaline oscillations (Figures 5a–5e), consistent with recent box model calculations [*Asmus et al.*, 1999]. We thus conclude that provided that our model accurately reflects ocean circulation, particle flux, and the behavior of ^{231}Pa and ^{230}Th in seawater, the current data rule out the possibility that the THC was totally shut off during the LGM. However, the possibility that THC was reduced to a level as low as 50% of its present strength cannot be dismissed (Figure 6a).

The model suggests that the mean $^{231}Pa/^{230}Th$ of the North Atlantic (7°N–80°N) is more sensitive to THC strength than the mean $^{231}Pa/^{230}Th$ of the whole Atlantic (47°S–80°N) (compare Figure 6b with Figure 6a). From our database the mean $^{231}Pa/^{230}Th$ of Holocene sediments from the North Atlantic is 0.067±0.006 (n = 70; Table 5). Removing the two samples from the upwelling region off West Africa, we obtain 0.065±0.005 (n = 68; Table 5). For the glacial North Atlantic we obtain 0.062±0.016 (n = 15; data from off West Africa included) or 0.052±0.006 (n = 13; data from off West Africa excluded). The change from the LGM to Holocene is thus

$$\Delta_{NA} = -0.005 \pm 0.014 \quad (14)$$

when data from off West Africa are included and

$$\Delta_{NA} = -0.013 \pm 0.011 \quad (15)$$

when data from off West Africa are excluded. The North Atlantic mean $^{231}Pa/^{230}Th$ at the LGM could thus not have been higher by 0.009 than the modern value. In our model the North Atlantic mean $^{231}Pa/^{230}Th$ increases by 0.014 (variable k_1) or 0.016 (constant k_1) for a twofold reduction in THC strength (Figure 6b). Our results suggest therefore that the glacial THC was more than half its present strength. Considering $^{231}Pa/^{230}Th$ data from North Atlantic sediments only thus better constrains the intensity of the glacial THC. Our model predicts that the THC strength would have to drop by ~ 30% (from 24 Sv to 16 Sv) to increase the North Atlantic mean $^{231}Pa/^{230}Th$ by 0.010 (variable k_1) or 0.011 (constant k_1). This suggests that the glacial THC could not have been reduced by more than ~ 30% of its present intensity.

4.3. Rapidity of $^{231}Pa/^{230}Th$ Changes

We finally use our model to examine whether the sediment $^{231}Pa/^{230}Th$ can record transient changes in the Atlantic thermohaline circulation, such as hypothesized, e.g., during the fast climatic oscillations of the last glacial period [*Broecker et al.*, 1985]. We con-

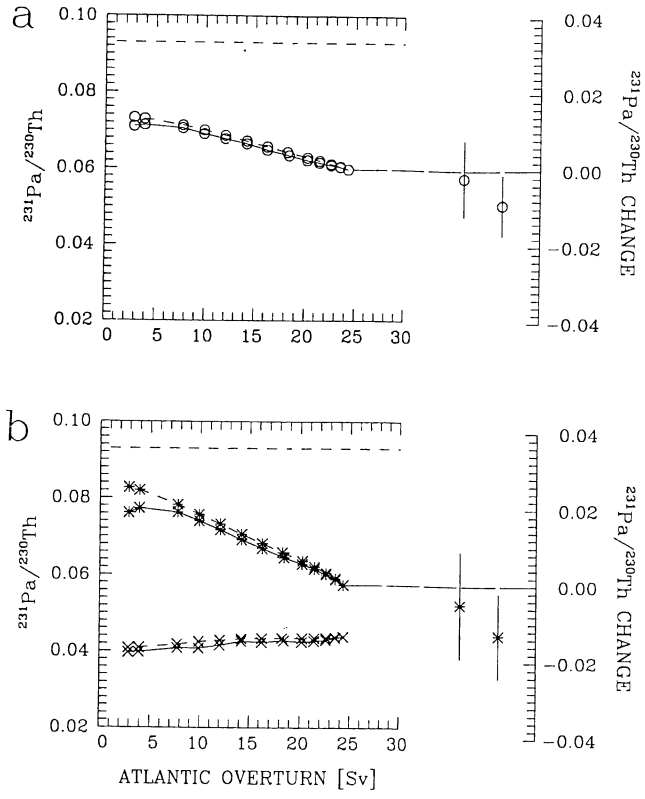

Figure 6. Basin mean $^{231}Pa/^{230}Th$ simulated for different THC strengths (on the left in Figures 6a–6b) compared to observational estimates of changes in basin mean $^{231}Pa/^{230}Th$ from the LGM to Holocene (on the right in Figures 6a–6b). The basin means simulated with variable and constant scavenging intensities are connected by a solid curve and a dashed curve, respectively. The observational estimates of changes in basin mean $^{231}Pa/^{230}Th$ (on the right in Figures 6a–6b) are calculated by including the high $^{231}Pa/^{230}Th$ values observed off West Africa (symbol on the left) and by excluding these values (symbol on the right). (a) Mean $^{231}Pa/^{230}Th$ of the whole Atlantic (model: 47°S–80°N; data: 45°S–80°N). (b) Mean $^{231}Pa/^{230}Th$ of the North Atlantic (asterisks; model and data: 7°N–80°N) and mean $^{231}Pa/^{230}Th$ of the South Atlantic (crosses; model: 47°–7°S). The zero on the scales for the observed $^{231}Pa/^{230}Th$ changes (right vertical scales) corresponds to the $^{231}Pa/^{230}Th$ simulated for modern circulation conditions, as shown by the horizontal long dashed line in Figures 6a–6b. This allows one to compare directly the modeled sensitivity of $^{231}Pa/^{230}Th$ to THC strength with the observational estimates of the changes in basin mean $^{231}Pa/^{230}Th$. The horizontal short dashed line on the left of Figures 6a–6b denotes the production ratio of the two radionuclides in the ocean water column.

sider two integrations where the THC is temporarily perturbed by a freshwater flux anomaly of different amplitude applied at the surface in the North Atlantic basin (Figure 7a). The anomaly is applied to an initial steady state corresponding to modern circulation conditions (as for the reference simulation) and constructed for freshwater perturbation experiments (for the procedure to construct the steady state, see *Marchal et al.* [1999]).

The Atlantic overturn drops from 24 Sv to a minimum of 12 or 3 Sv, depending on the prescribed anomaly (Figure 7b). The response of $^{231}Pa/^{230}Th$ to the fast THC changes is largest in the North Atlantic (Figure 7c), lowest in the South Atlantic (Figure 7d), and intermediate in the Southern Ocean (Figure 7e). The peak-to-peak amplitudes in the North Atlantic (at 50°N) amount to 0.016–0.030, increasing with the severity of the THC change (Figure 7c). The two latter values are larger than 75 and 90% of the analytical uncertainties reported for Holocene sediments [*Walter et al.*, 1999], respectively. Furthermore, recent measurements based on inductively coupled, plasma mass spectrometry typically constrain $^{231}Pa/^{230}Th$ at ±0.0025 (R. François et al., unpublished data, 1999). Our results thus suggest that high-resolution $^{231}Pa/^{230}Th$ records from North Atlantic cores with high deposition rates could document the fast changes of the THC that probably punc-

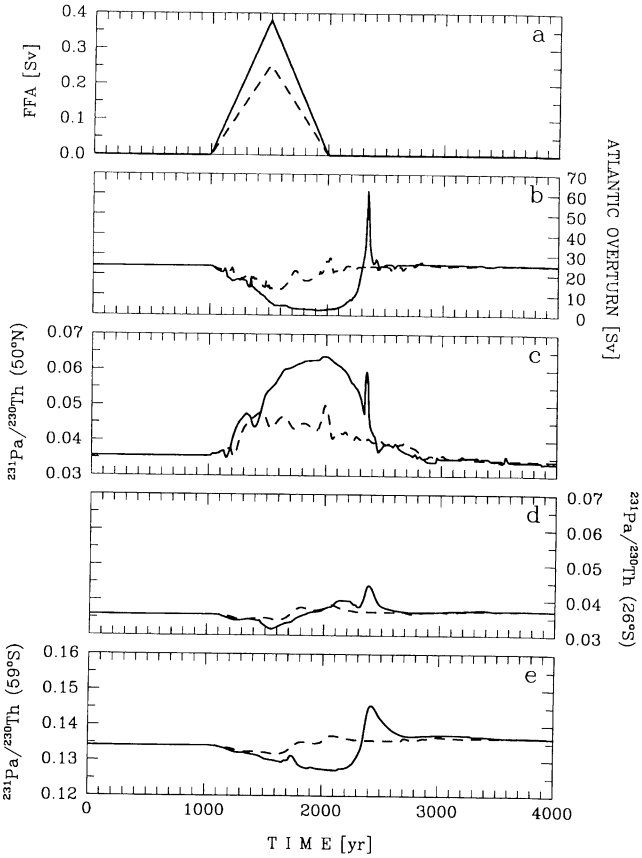

Figure 7. Time series from two different model experiments of freshwater flux anomaly (FFA). The two experiments are characterized by a different amplitude of the FFA applied at the same location in the North Atlantic (between 32.5° and 45°N). The time series illustrate (a) the FFA, (b) the Atlantic thermohaline overturn, and (c–e) the sediment $^{231}Pa/^{230}Th$ ratio in the Atlantic at 50°N and 26°S and in the Southern Ocean at 59°S.

tuated the last glaciation (see also box model calculations by *Yu et al.* [1996, Figure 5]).

5. Discussion

Our model results support the view that the ratio between ^{231}Pa and ^{230}Th in Atlantic sediments could be used to constrain past changes in the strength of the Atlantic thermohaline circulation [*Yu et al.*, 1996]. *Yu et al.* [1996], however, did not consider the effect of enhanced ^{231}Pa scavenging by biogenic opal south of the polar front on the ^{231}Pa budget of the South Atlantic. As a consequence, they probably overestimated the effect of the THC on the mean $^{231}Pa/^{230}Th$ of the entire Atlantic. Our results suggest that the current uncertainties in Atlantic mean $^{231}Pa/^{230}Th$ cannot rule out a 50% decrease in THC at the Last Glacial Maximum. Hence the conclusion of *Yu et al.* [1996] that the intensity of the THC during the LGM and Holocene was "similar", must be revisited.

We find that the mean $^{231}Pa/^{230}Th$ of the North Atlantic is more sensitive to THC changes than the mean $^{231}Pa/^{230}Th$ of the entire Atlantic. If we use the former ratio instead of the latter, we thus better constrain changes in large-scale Atlantic overturn and find that the THC at the LGM could not have been reduced below 70% of its present strength. This reduction level would be consistent with a recent reconstruction of the geostrophic transport in the Florida Straits [*Lynch-Stieglitz et al.*, 1999]. The uncertainties in North Atlantic mean $^{231}Pa/^{230}Th$ are still very large, however, to the point that it is also consistent with a larger than modern intensity of the THC at the LGM. This latter possibility seems unlikely, when considering the results from other paleocirculation tracers [*Boyle*, 1992, 1995; *Lynch-Stieglitz et al.*, 1999].

We discuss below the potential effects on our results of (1) opal production outside the Southern Ocean and (2) enhanced boundary scavenging in the glacial Atlantic. Opal production outside the Southern Ocean may affect $^{231}Pa/^{230}Th$ in the Atlantic and Southern Ocean. Estimating opal production in marine surface waters from the amount of opal in underlying sediments is confounded by the many factors that can influence the efficiency of opal preservation [*Broecker and Peng*, 1982; *Spencer*, 1983; *Archer et al.*, 1993]. Nevertheless, the distribution of opal in marine sediments points to the Southern Ocean, the equatorial Pacific, and the northernmost Pacific as the major regions of opal production in the open ocean [*Broecker and Peng*, 1982; *Spencer*, 1983]. We have repeated the equilibrium simulations with a vigorous (24 Sv), intermediate (12 Sv), and collapsed THC strength (3 Sv) by adding an opal production of 13 Tmol Si yr^{-1} (the same as in the Southern Ocean for modern circulation conditions) both in the equatorial (7.5°S–7.5°N) and northern North Pacific (45°–55°N). The difference between the $^{231}Pa/^{230}Th$ in the Atlantic and Southern Ocean predicted without and with this additional production does not exceed 0.003. Furthermore, the changes in Atlantic and North Atlantic mean $^{231}Pa/^{230}Th$ predicted for the full (0.011 and 0.019, respectively) and twofold reduction of the THC (0.008 and 0.014) are identical to those predicted when opal production outside the Southern Ocean is omitted. This production does not therefore alter the Atlantic ^{231}Pa deficit and Southern Ocean ^{231}Pa excess and their sensitivity to THC changes in our model.

Boundary scavenging, on the other hand, may have been enhanced in the glacial Atlantic, which could also affect our results. As mentioned above, the current database suggests that boundary scavenging of Pa in the Holocene Atlantic is weak [*Yu et al.*, 1996, Figure 2b; *Walter et al.*, 1999, Figure 5]. Most of the Holocene $^{231}Pa/^{230}Th$ data for the Atlantic's margins come from the Middle Atlantic Bight [*Yu et al.*, 1996, Figure 2b]. The $^{231}Pa/^{230}Th$ data from this region were obtained on young sediments from 20 different cores [*Anderson et al.*, 1994]. None of these $^{231}Pa/^{230}Th$ values is significantly larger than 0.093 [*Anderson et al.*, 1994, Table 2]. Furthermore, only two cores from the upwelling region off West Africa, one of the Atlantic regions where boundary scavenging would be most pronounced, have a $^{231}Pa/^{230}Th$ larger than the production ratio (e.g., Figure 4a). This contrasts sharply with the eastern equatorial Pacific, where $^{231}Pa/^{230}Th$ is consistently $>$ 0.093 [*Walter et al.*, 1999, Figure 4]. On the other hand, there are only three cores from off West Africa, which document boundary scavenging during the LGM [*Yu et al.*, 1996, Figure 2b]. The indication for enhanced boundary scavenging in the glacial Atlantic is thus very weak.

Such an enhancement, however, would be consistent with our current understanding of the oceanic behavior of ^{231}Pa if the THC was indeed reduced at the LGM and deserves therefore consideration. Since boundary scavenging is not incorporated in our zonally averaged model, we have compared above the model results with the changes in basin mean $^{231}Pa/^{230}Th$ from the LGM to Holocene calculated either by including or by excluding the high values from off West Africa. Another possibility would have been to use a model that can represent boundary scavenging. One major difficulty here is that boundary scavenging may occur on small spatial scales, so that high-resolution models must be used to represent this effect properly (*Henderson et al.* [1999] pointed out that boundary scavenging is not explicitly incorporated in their coarse-resolution, 3-D model).

We therefore can only speculate about the qualitative effect of a possible enhancement of boundary sca-

venging in the glacial Atlantic. The ^{231}Pa excess that would reside in this basin in response to reduced NADW flux to the Southern Ocean should be at least partly trapped at the margins. Accordingly, the sensitivity of the sediment $^{231}Pa/^{230}Th$ in the open Atlantic would be lessened. This points to the necessity to better document $^{231}Pa/^{230}Th$ of Holocene and LGM sediments at the Atlantic's margins and to account for the possible emergence of boundary scavenging when interpreting the changes in basin mean $^{231}Pa/^{230}Th$ between different climatic periods.

We finally examine whether the Atlantic $^{231}Pa/^{230}Th$ can still constrain the THC strength at the LGM, considering (1) the possibility that this reduction was short-lived and (2) the effect of bioturbation on the sediment $^{231}Pa/^{230}Th$ records. We have applied a linear symmetric filter (simple moving averages) with different time windows to the changes in Atlantic mean $^{231}Pa/^{230}Th$ predicted for the transient collapse of the THC from 24 to 3 Sv (section 4.3). The peak-to-peak amplitude in Atlantic mean $^{231}Pa/^{230}Th$ amounts to 0.015 (time window is 200 and 400 years), 0.014 (600 years), 0.013 (800 years), and 0.011 (1000 years). All these values are larger than the upper bound of +0.008 for the observed change in Atlantic mean $^{231}Pa/^{230}Th$ from the LGM to Holocene. Our previous conclusion that this change rules out a complete collapse of the THC at the LGM remains therefore valid. However, the exercise shows that the smoothing effect of bioturbation on Atlantic $^{231}Pa/^{230}Th$ records can be significant and may require the use of sediment cores with sufficient accumulation rates in order to constrain the THC at the LGM. We note that the sediment $^{231}Pa/^{230}Th$ should not be sensitive to events lasting for periods much shorter than the residence time of Pa in deep water ($\sim$ 200 years), not because of bioturbation but because of the response time of seawater Pa to circulation changes.

6. Outlook

Several possibilities present themselves to increase the potential of the sediment $^{231}Pa/^{230}Th$ to document past changes of the THC. First, the spatial coverage in the North Atlantic, data quality, and time resolution of the sediment $^{231}Pa/^{230}Th$ database should be increased. The spatial coverage of deep-sea cores must be enhanced in order to clearly delineate oceanic regions with possible distinct $^{231}Pa/^{230}Th$. There is an obvious lack of data from high-productivity areas in the Atlantic that might be a sink for Pa, which implies a high uncertainty in the basin mean $^{231}Pa/^{230}Th$. Reducing analytical and stratigraphic errors, on the other hand, should improve the data quality. Recent progress in mass spectrometric techniques [*Shaw and François*, 1991; *Yu*, 1994], the increasing availability of cores with undisturbed surfaces and accurate stratigraphy, and studies on the effect of particle composition on $^{231}Pa/^{230}Th$ [*Walter et al.*, 1997; *Luo and Ku*, 1999] should be extended.

Second, it is important that our results be confirmed by other models including a more complete description of both the deep-ocean circulation and trace metal scavenging. The major weakness of our approach is the use of a zonally averaged model with coarse resolution and flat bottom to determine the sensitivity of the sediment $^{231}Pa/^{230}Th$ to the THC. A natural followup to this study is thus the use of 3-D ocean circulation models with high spatial resolution and realistic bathymetry to constrain this sensitivity in different oceanic regions (for a first step in this direction, see *Henderson et al.* [1999]). While the models will help us to better interpret the distribution of ^{231}Pa and ^{230}Th in the water column and sediment, synergistically, our rapidly expanding database will also prove useful for better constraining deep water circulation and particle flux in the models. Both approaches must be pursued in parallel to iteratively converge toward a better representation and understanding of the glacial ocean.

Acknowledgments. This study was made possible by the Swiss National Science Foundation and the Federal Office of Science and Education. We thank M. Frank, C. Heinze, G. Henderson, A. Mangini, M. Rutgers van der Loeff, and one anonymous reviewer for useful comments and F. von Blanckenburg for discussions.

References

Anderson, H., R. François, and S. B. Moran, Experimental evidence for differential adsorption of Th and Pa on different solid phases in seawater, *Eos Trans. AGU, 73*(43), *Fall Meet. Suppl.*, 270, 1992.

Anderson, R. F., M. P. Bacon, and P. G. Brewer, Removal of ^{230}Th and ^{231}Pa from the open ocean, *Earth Planet. Sci. Lett., 62*, 7–23, 1983a.

Anderson, R. F., M. P. Bacon, and P. G. Brewer, Removal of ^{230}Th and ^{231}Pa at ocean margins, *Earth Planet. Sci. Lett., 66*, 73–90, 1983b.

Anderson, R. F., M. Q. Fleisher, P. E. Biscaye, N. Kumar, B. Dittrich, P. Kubik, and M. Suter, Anomalous boundary scavenging in the Middle Atlantic Bight: Evidence from ^{230}Th, ^{231}Pa, ^{10}Be and ^{210}Pb, *Deep Sea Res., Part II, 41*, 537–561, 1994.

Archer, D., M. Lyle, K. Rodgers, and P. Froelich, What controls opal preservation in tropical deep-sea sediments?, *Paleoceanography, 8*, 7–21, 1993.

Asmus, T., M. Frank, C. Koschmieder, N. Frank, R. Gersonde, G. Kuhn, and A. Mangini, Variations of biogenic particle flux in the southern Atlantic section of the Subantarctic Zone during the late Quaternary: Edivence from sedimentary $^{231}Pa_{ex}$ and $^{231}Th_{ex}$, *Mar. Geol., 159*, 63–78, 1999.

Bacon, M. P., Tracers of chemical scavenging in the ocean: Boundary effects and large scale chemical fractionation, *Philos. Trans. R. Soc. London, Ser. A, 320*, 187–200, 1988.

Bacon, M. P., and R. F. Anderson, Distribution of thorium isotopes between dissolved and particulate forms in the deep sea, *J. Geophys. Res., 87*, 2045–2056, 1982.

Bacon, M. P., and J. N. Rosholt, Accumulation rates of ^{230}Th and ^{231}Pa and some transition metals on the Bermuda Rise, *Geochim. Cosmochim. Acta, 46*, 651–666, 1982.

Boyle, E. A., Cadmium and $\delta^{13}C$ paleochemical ocean distributions during the stage 2 glacial maximum, *Annu. Rev. Earth Planet. Sci., 20*, 245–287, 1992.

Boyle, E. A., Last-Glacial-Maximum North Atlantic Deep Water: On, off or somewhere in-between?, *Philos. Trans. R. Soc. London, Ser. B, 348*, 243–253, 1995.

Boyle, E. A., Deep water distillation, *Nature, 379*, 679–680, 1996.

Broecker, W. S., A revised estimate for the radiocarbon age of North Atlantic Deep Water, *J. Geophys. Res., 84*, 3218–3226, 1979.

Broecker, W. S., and T.-H. Peng, *Tracers in the Sea*, Lamont-Doherty Earth Obs., Palisades, N. Y., 1982.

Broecker, W. S., D. Peteet, and D. Rind, Does the ocean-atmosphere system have more than one stable mode of operation?, *Nature, 315*, 21–25, 1985.

Chen, J. H., R. L. Edwards, and G. J. Wasserburg, ^{238}U, ^{234}U and ^{232}Th in seawater, *Earth Planet. Sci. Lett., 80*, 241–251, 1986.

Colley, S., J. Thomson, and P. P. Newton, Detailed ^{230}Th, ^{232}Th, and ^{210}Pb fluxes recorded by the 1989/90 BOFS sediment trap time-series at 48°N, 20°W, *Deep Sea Res., Part I, 42*, 833–848, 1995.

DeMaster, D. J., The marine budget of silica and ^{32}Si, Ph.D. thesis, Yale Univ., New Haven, Conn., 1979.

Dudewicz, E. J., and S. N. Mishra, *Modern Mathematical Statistics*, John Wiley, New York, 1988.

England, M. H., On the formation of Antarctic Intermediate and Bottom Water in ocean general circulation models, *J. Phys. Oceanogr., 22*, 918–926, 1992.

Henderson, G. M., C. Heinze, R. F. Anderson, and A. M. E. Winguth, Global distribution of the ^{230}Th flux to ocean sediments constrained by GCM modelling, *Deep Sea Res., Part I, 46*, 1861–1894, 1999.

Honjo, S., Material fluxes and modes of sedimentation in the mesopelagic and bathypelagic zones, *J. Mar. Res., 38*, 53–97, 1980.

Honjo, S., S. J. Manganini, and L. J. Poppe, Sedimentation of lithogenic particles in the deep ocean, *Mar. Geol., 50*, 199–219, 1982.

Krishnaswami, S., D. Lal, B. L. K. Somayajulu, R. F. Weiss, and H. Craig, Large-volume in-situ filtration of deep Pacific waters: Mineralogical and radioisotope studies, *Earth Planet. Sci. Lett., 32*, 420–429, 1976.

Krishnaswami, S., M. M. Sarin, and B. L. K. Somayajulu, Chemical and radiochemical investigations of surface and deep particles of the Indian Ocean, *Earth Planet. Sci. Lett., 54*, 81–96, 1981.

Ku, T.-L., Uranium series disequilibrium in deep-sea sediments, Ph.D. thesis, Columbia Univ., New York, 1966.

Ku, T.-L., J. L. Bischoff, and A. Boersma, Age studies of Mid-Atlantic Ridge sediments near 42°N and 20°N, *Deep Sea Res., 19*, 233–247, 1972.

Kumar, N., Trace metals and natural radionuclides as tracers of ocean productivity, Ph.D. thesis, Columbia Univ., New York, 1994.

Kumar, N., R. Gwiozda, R. F. Anderson, and P. N. Froelich, $^{231}Pa/^{230}Th$ ratios in sediments as a proxy for past changes in Southern Ocean productivity, *Nature, 362*, 45–48, 1993.

Lao, Y., R. F. Anderson, W. S. Broecker, S. E. Trumbore, H. J. Hofmann, and W. Wolfli, Transport and burial rates of ^{10}Be and ^{231}Pa in the Pacific Ocean during the Holocene period, *Earth Planet. Sci. Lett., 113*, 173–189, 1992.

Lea, D. W., A trace metal perspective on the evolution of Antarctic Circumpolar Deep Water chemistry, *Paleoceanography, 10*, 733–747, 1995.

Legeleux, F., Relation entre particules marines et message sédimentaire: Flux de matière dans la colonne d'eau et transformations à l'interface eau-sédiment dans l'Océan Atlantique tropical de nord-est, Ph.D. thesis, Univ. of Paris, Paris, 1994.

Luo, S., and T.-L. Ku, Oceanic $^{231}Pa/^{230}Th$ ratio influenced by particle composition and remineralization, *Earth Planet. Sci. Lett., 167*, 183–195, 1999.

Luo, S., T.-L. Ku, M. Kusakabe, J. K. B. Bishop, and Y.-L. Yang, Tracing particle cycling in the upper ocean with ^{230}Th and ^{228}Th: An investigation in the equatorial Pacific along 140°W, *Deep Sea Res., Part II, 42*, 805–829, 1995.

Lynch-Stieglitz, J., W. B. Curry, and N. Slowey, Weaker Gulf Stream in the Florida Straits during the Last Glacial Maximum, *Nature, 402*, 644–648, 1999.

Mangini, A., and L. Dieter-Haass, Excess ^{230}Th in sediments off NW Africa traces upwelling in the past, in *Coastal Upwelling: Its Sedimentary Record*, edited by J. Thiede and E. Suess, pp. 455–470, Plenum, New York, 1983.

Marchal, O., T. F. Stocker, and F. Joos, A latitude-depth, circulation-biogeochemical ocean model for paleoclimate studies. Development and sensitivities, *Tellus, Ser. B, 50*, 290–316, 1998.

Marchal, O., T. F. Stocker, and F. Joos, Physical and biogeochemical responses to freshwater-induced thermohaline variability in a zonally averaged ocean model, in *Mechanisms of Global Climate Change at Millennial Time Scales*, Geophys. Monogr. Ser., vol. 112, pp. 263–284, edited by R. Webb, P. U. Clark, and L. D. Keigwin, AGU, Washington, D. C., 1999.

Moore, W. S., The thorium isotope content of ocean water, *Earth Planet. Sci. Lett., 53*, 419–426, 1981.

Moran, S. B., M. A. Charette, J. A. Hoff, R. L. Edwards, and W. M. Landing, Distribution of ^{230}Th in the Labrador Sea and its relation to ventilation, *Earth Planet. Sci. Lett., 150*, 151–160, 1997.

Nelson, D. M., and L. I. Gordon, Production and pelagic dissolution of biogenic silica in the Southern Ocean, *Geochim. Cosmochim. Acta, 46*, 491–501, 1982.

Nelson, D. M., P. Tréguer, M. A. Brzezinski, A. Leynaert, and B. Quéguiner, Production and dissolution of biogenic silica in the ocean: Revised global estimates, comparison with regional data and relationship to biogenic sedimentation, *Global Biogeochem. Cycles, 9*, 359–372, 1995.

Nozaki, Y., and Y. Horibe, Alpha-emitting thorium isotopes in northwest Pacific deep waters, *Earth Planet. Sci. Lett., 65*, 39–50, 1983.

Nozaki, Y., and T. Nakanishi, ^{231}Pa and ^{230}Th profiles in the open ocean water column, *Deep Sea Res., 32*, 1209–1220, 1985.

Nozaki, Y., Y. Horibe, and H. Tsubota, The water column distributions of thorium isotopes in the western North Pacific, *Earth Planet. Sci. Lett., 54*, 203–216, 1981.

Nozaki, Y., H.-S. Yang, and M. Yamada, Scavenging of thorium in the ocean, *J. Geophys. Res., 92*, 772–778, 1987.

Rosenthal, Y., E. A. Boyle, and L. Labeyrie, Last Glacial Maximum paleochemistry and deepwater circulation in the Southern Ocean: Evidence from foraminiferal cadmium, *Paleoceanography, 12*, 787–796, 1997.

Roy-Barman, M., J. H. Chen, and G. J. Wasserburg, ^{230}Th–^{232}Th systematics in the central Pacific Ocean: The sources and fates of thorium, *Earth Planet. Sci. Lett., 139*, 351–363, 1996.

Rutgers van der Loeff, M. M., and G. W. Berger, Scavenging of ^{230}Th and ^{231}Pa near the Antarctic Polar Front in the South Atlantic, *Deep Sea Res., Part I, 40*, 339–357, 1993.

Scholten, J. C., M. M. Rutgers van der Loeff, and A. Michel, Distribution of ^{230}Th and ^{231}Pa in the water column in relation to the ventilation of the deep Arctic basins, *Deep Sea Res., Part II, 42*, 1519–1531, 1995.

Shaw, T. J., and R. François, A fast and sensitive ICP-MS assay for the determination of ^{230}Th in marine sediments, *Geochim. Cosmochim. Acta, 55*, 2075–2078, 1991.

Spencer, C. P., Marine biogeochemistry of silicon, in *Silicon Geochemistry and Biogeochemistry*, edited by S. R. As-

ton, pp. 101–141, Academic, San Diego, Calif., 1983.

Stocker, T. F., and D. G. Wright, Rapid changes in ocean circulation and atmospheric radiocarbon, *Paleoceanography, 11*, 773–796, 1996.

Stocker, T. F., D. G. Wright, and W. S. Broecker, The influence of high-latitude surface forcing on the global thermohaline circulation, *Paleoceanography, 7*, 529–541, 1992.

Stuiver, M., P. D. Quay, and H. G. Ostlund, Abyssal water carbon-14 distribution and the age of the world oceans, *Science, 219*, 849–851, 1983.

Vogler, S., J. Scholten, M. Rutgers van der Loeff, and A. Mangini, ^{230}Th in the eastern North Atlantic: The importance of water mass ventilation in the balance of ^{230}Th, *Earth Planet. Sci. Lett., 156*, 61–74, 1998.

Walter, H. J., M. M. Rutgers van der Loeff, and H. Hoeltzen, Enhanced scavenging of ^{231}Pa relative to ^{230}Th in the South Atlantic south of the Polar Front: Implications for the use of the $^{231}Pa/^{230}Th$ ratio as a paleoproductivity proxy, *Earth Planet. Sci. Lett., 149*, 85–100, 1997.

Walter, H.-J., M. M. Rutgers van der Loeff, and R. François, Reliability of the $^{231}Pa/^{230}Th$ activity ratio as a tracer for bioproductivity of the ocean, in *Use of Proxies in Paleoceanography: Examples from the South Atlantic*, edited by G. Fischer and G. Wefer, pp. 393–408. Springer-Verlag, New York, 1999.

Wollast, R., The silica problem, in *The Sea*, vol. 5, edited by E. D. Goldberg, pp. 359–392, J. Wiley, New York, 1974.

Wright, D. G., and T. F. Stocker, Sensitivities of a zonally averaged global ocean circulation model, *J. Geophys. Res., 97*, 12,707–12,730, 1992.

Yang, H.-S., Y. Nozaki, H. Sakai, and A. Masuda, The distribution of ^{230}Th and ^{231}Pa in the deep-sea surface sediments of the Pacific Ocean, *Geochim. Cosmochim. Acta, 50*, 81–89, 1986.

Yu, E.-F., Variations in the particulate flux of ^{230}Th and ^{231}Pa and paleoceanographic applications of the $^{231}Pa/^{230}Th$ ratio, Ph.D. thesis, Woods Hole Oceanogr. Inst., Woods Hole, Mass., 1994.

Yu, E.-F., R. François, and M. P. Bacon, Similar rates of modern and last-glacial ocean thermohaline circulation inferred from radiochemical data, *Nature, 379*, 689–694, 1996.

R. François, Department of Marine Chemistry and Geochemistry, Woods Hole Oceanographic Institution, Woods Hole, MA 02543. (e-mail: rfrancois@whoi.edu)

F. Joos, O. Marchal, and T. F. Stocker, Climate and Environmental Physics Physics Institute, University of Bern, Sidlerstrasse 5, CH-3012 Bern, Switzerland. (e-mail: joos@climate.unibe.ch; marchal@climate.unibe.ch; stocker@climate.unibe.ch)

(Received January 3, 2000;
revised June 27, 2000;
accepted July 25, 2000.)